Anomalous dielectric constant value of graphene oxide/Polyvinyl alcohol thin film

Abd Elhamid M. Abd Elhamid, Heba Shawkey, Amr Nada, Mikhael Bechelany

Anomalous dielectric constant value of graphene oxide/Polyvinyl alcohol thin film

Abd Elhamid M. Abd Elhamid[a,b] , Heba A. Shawkey[b,c], Amr A. Nada[d,e,*], Mikhael Bechelany[e]

[a] Department of Laser Sciences and Interactions, National Institute of Laser Enhanced Sciences, Cairo University, Egypt.

[b] Nanotechnology Lab., Electronics Research Institute (ERI), Cairo, Egypt.

[c] Microelectronics department, Electronics Research Institute (ERI), Egypt.

[d] Dept. of Analysis and Evaluation, Egyptian Petroleum Research Institute, Cairo, Nasr city P.B. 11727, Egypt.

[e] Institut Européen des Membranes, UMR 5635, Université Montpellier, CNRS, ENSCM, Place Eugene Bataillon, F-34095 Montpellier cedex 5, France.

Corresponding authors: Amr A. Nada (amr.nada@umontpellier.fr).

Abstract

Graphene oxide/polyvinyl alcohol (GO/PVA) composites have been developed using facile colloidal processing technique to form a super dielectric spacer of 10^6 order. The dielectric characteristics of GO/PVA composite were investigated at a frequency range from 20 Hz to 1 M Hz. The electrical analysis showed a complex interaction that vary from Debye and could be explained using Bruggeman and Maxwell-Garnett assumptions in the high-frequency range and Percolation theory in the low range. Due to the ageing effect and the observed high imaginary part, an investigation of GO film dielectric properties were investigated. The results incorporate a crucial role of water contents on corresponding GO and GO/PVA electromagnetic interaction besides the well-established functional group's theory. Transmission electron microscopy, X-ray diffraction, dispersive Raman, potentiostat/galvanostat and LCR meter were utilized to perform microscopic, structure and electrical characterizations.

Keywords: Graphene oxide, super dielectric material, PVA, ordinary capacitor, cyclic voltammetry.

Introduction

High- k material where "k" the dielectric constant (DiC) is an important component to achieve high capacitance. Those materials are required to reduce dimensions of integrated circuits (IC) and enhance operation frequency as well. Therefore, those materials are needed for the dielectric gate in complementary metal oxide semiconductor ICs, non-volatile static memory devices, and storage capacitors [1–4]. Although, most polymers are lightweight, scalable and low cost, however, most of them have relatively low DiCs. Thereupon, nano-composites proved to be an effective technique in enhancing dielectric properties by filling polymers [5]. Graphitic-polymers composites have attracted much attention recently because of good electrical and mechanical properties [6–8]. Therefore, carbon-based material is a backbone for a wide band of application especially energy storage systems [9–11]. Among carbon materials, Graphene oxide (GO), a pseudo-two-dimensional hexagonal carbon structure with oxygen functional groups [12], which is used in several applications such as capacitors, optoelectronics, memory devices, photocatalysis and drug delivery [13–17]. GO is famous for being prepared through hummer chemical method by using acidic medium and high oxidation agent [18–22]. Moreover, GO is a scalable technique to produce reduced graphene oxide and have a wide band of applications. Polymer/GO composites would be interesting to develop cheap and eco-friendly materials that are suitable for several technological applications [23,24].

Interestingly, GO was reported to have high DiC in the order of 10^4 [25] and even higher of 10^6 order [26]. On the contrary, Kavinkumar *et al.* [27] reported a small DiC value of about ~17 and

even much lower value was reported by Saloma *et al.* [28]. The difference in previously reported of DiC values need further investigation in order to define the other parameters.

In the present work, high weight ratios of GO to Polyvinyl alcohol (PVA) nanocomposites were prepared then coated on Aluminum foil (Al). A two plate ordinary capacitors were fabricated and characterized. Moreover, crude GO and treated GO film at 100 °C were used as spacers in other ywo double plates capacitors in order to study DiC value of different GO spacers.

Experimental

Dark brown GO powder was prepared using the improved hummers method [22,29]. In the typical experiment, graphite (5 g), $NaNO_3$ (2.5 g) and H_2SO_4 (115 ml) were mixed and stirred in an ice bath for half an hour. Subsequently, 15 g of $KMnO_4$ were added slowly. The reaction mixture was warmed to 40 °C and stirred for another 30 min. DI Water (230 ml) was added slowly then the temperature was increased to 98 °C and it was stirred for 30 min. Finally, 500 ml of DI water were added, followed by the dropwise adding of 50 ml (30% H_2O_2). After filtering and washing several times, 100 ml of 0.1 M HCl was added and left for 24 h. The GO was washed several times with DI water then centrifuged, collected and dehydrated at 60 °C for 24 h in a vacuum oven. It's worth to mention that, the analytical grade chemicals were purchased from Sigma Aldrich and used without further purification.

One gram of GO powder was dispersed in 100 ml of DI water for 2 hours to obtain highly exfoliated graphene oxide using the ultrasonic probe. In this meanwhile, 8% PVA was prepared by dissolving 8 g in 100 ml DI water at 85 °C under reflux and rapid stirring. GO/PVA composites at weight ratios of 10%, 20% and 50% were prepared via a facile colloidal processing technique. 10 ml of PVA aqueous solution was added to the 3 different amounts of GO suspended solutions

and the mixture was stirred gently for 6 h under reflux to ensure forming a uniform dispersion of GO in the PVA matrix. 80 μm commercial Al foils were cut into 4×5 cm^2 then cleaned by DI, ethanol and acetone, respectively. Subsequently, a layer of the mixture was coated on the Al foils then dehydrated for 60 min till forming a thin rigid film. The final GO/PVA sandwiched interlayer between the attached Al foils was set to a thickness of about 500 μm after dehydrating at 60 ^{o}C for 12h in vacuum. The two plates were attached together using 50 μml of the composite suspension then gently compressed for 24h to achieve good stacking (the estimated thickness after this step was ~475 μm). Eventually, the different ratio of GO/PVA capacitors was dehydrated for 24h at 60 ^{o}C in vacuum.

The GO suspension was casted on Al foil as the main substrate that contains 500 nm of sputtered Ag on its surface, the GO film thickness was ~10 μm. After dehydration at RT for 24h, a shadow mask was used to sputter another 500 nm of Ag on the GO surface. The two samples were conducted to 2 different treatment conditions in vacuum, one of them was at 60 ^{o}C (crude GO) while the other was at 100 ^{o}C (dehydrated GO).

Capacitance values of the fabricated capacitors were measured using (Agilent E4980A/20-2 MH/precision LCR meter) whereas cyclic voltammetry (CV) at different scan rates curves were performed using (VSP-300 Bio-Logic). GO, GO dehydrated films on glass substrates were characterized using X-ray diffraction XRD (X'Pert Pro) and dispersive Raman microscopy with a laser source of 532 nm at a power of 10 mW (Bruker Senterra). The green laser was focused onto the sample with an optical microscope using a 100X lens. TEM images were monitored using JEM-2100 Plus.

Result and Discussion

The different ratios of GO/PVA double plate capacitors were measured using C-R parallel mode at different frequencies started from 20 Hz to 1 MHz The dielectric constant of the fabricated capacitors was estimated using equation (1) to identify dimensional independent DiC value,

$$C = \varepsilon_0 \varepsilon_r \, A/d \tag{1}$$

where C is the capacitance (F), A represents the metal foil area (m^2), ε_r is the DiC value while ε_0 is the vacuum electric permittivity ($\varepsilon_0 \approx 8.854 \times 10^{-12}$ F·m^{-1}); and d is the separation between the plates in meter.

The estimated dielectric constants of GO/PVA composites of 10%, 20% and 50% weight ratios are shown in Fig.1 (a). At the low frequency, the whole values are located within 10^6 order. However, they appeared to fall down in a steeper manner along with frequency upturn which is in good agreement with previous experimental [24,30]. During slow rate of the oscillating electric field, relatively induced and permanent dipoles have sufficient time to align themselves along the applied electric field direction leading to enhanced polarization. On the other hand, the composites polar molecules rotational motion would not be quick enough to retrieve equilibrium with the rapidly oscillating applied electric field. Moreover, terms such as orientation, ionic and space charge that contributions dielectric value are eliminated during frequency increase [25,26].

Thereupon, the 20% GO/PVA composite ratio exhibits the highest dielectric constant at frequencies lower than 1KHz but thereafter overtaken by the 10% GO/PVA composite ratio. In addition, the 50% composite reveals the lowest dielectric constant along with the applied frequency presumably due to the formation of GO large clusters within the polymer matrix. Although of GO flakes functional groups that would enhance the dielectric constant effectively, the exact electric field interaction mechanism is unknown. The significant enhanced DiC of GO/PVA composites at the first sight could be attributed to Maxwell-Wagner- Sillar (MWS) effect

[25][26], interfacial polarization between GO fillers inside PVA polymer [30] and functional group contribution [26]. Although the 50% GO/PVA ratio is expected to have the highest water contents, it presented the lowest DiC value and could be attributed to the high GO load that promotes the high rate of water loss during dehydration process and overfill the polymer matrix.

The frequency dependence of the composite films is governed by the equation of motion. As the resonance frequency $\varepsilon``$ peak appeared at low frequency, a sharp drop is expected at higher oscillation rate. The relaxation responses of the GO/PVA spacers could be attributed to complex interactions that cause associated fluctuations between different quantum states. Accordingly, an associated delay is initiated in returning the absorbed energy within dipoles to electromagnetic wave again which attenuate the dielectric response [31].

The GO/PVA composites contain bounded charges susceptible to the displacement polarization as well as free charges responsible for DC conductivity. Thereupon, the GO/PVA parallel plate capacitor will be treated as a parallel RC circuit with phase angle given by equation (2)

$$\theta = \tan^{-1}(I_C/I_R) \tag{2}$$

, where I_R and I_c are the resistive and capacitive currents, respectively. Fig.1 (b) shows the phase angle dispersion of different ratios GO/PVA composites versus frequency. Capacitor quality factor and current flowing through the spacer is associated with phase angle value. Thereupon, the 10% GO/PVA ratio possess the best spacer performance. It is believed that the performance could be enhanced much further by reducing contamination, ions and water contents through efficient dehydration process and high oxidation degree of GO. The phase angle measurements showed that 10% ratio has the highest quality due to owing the lowest trapped water contents allied with GO weight ratio. Whereas, the 50% sample showed the lowest phase angle due to the GO clustering that promotes current flow through the spacer as a result of conductive graphitic defects.

While the real DiC part is an indication to which material can store the electric field through polarization, the imaginary part ($\varepsilon``$) is directly conducted to energy dissipation into heat. Therefore, the imaginary DiC values versus frequency are presented in Fig. 1 (c). The three different weight ratios drop with frequency demonstrating frequency-dependent typical characteristic with very low-frequency relaxation bump [32]. The high losses could be attributed to GO defects, conductive defects, water contents and ions residuals [25,26,32].

On the other hand, complex dielectric susceptibility curve (Cole-Cole) is shown in Fig.1 (d) to enable a better understanding of the dielectric properties, where ε is the complex permittivity, $\varepsilon`$ real value and $\varepsilon``$ represent the imaginary part. The pure Debye behaviour could be defined as a single relaxation time based on non-interacting ideal dipoles could not be applied due to the complex composite structure [33]. As a result of several functional groups, defects, intercalated water molecules and associated interactions, GO/PVA film will serve as a complex time response spacer. Therefore, the Cole-Cole plot presents such complex shapes that vary with the GO weight ratio. In addition, it is hard to be described as a collective semi-circular shape. The GO/PVA spacers could be described according to Percolation theory, where probabilistic assumption describe the filler geometry distribution within the polymer matrix and electromagnetic interaction of flakes, polymer and flakes/polymer at low-frequency [34]. Bruggeman and Maxwell-Garnett theories could be applied in the high-frequency [35]. As the GO weight ratio increases, the interspacing between flakes that are filled with PVA decreases and leads to maximize the impact of GO flakes complex response to the applied electric field. Although the lowest used weight ratio was 10%, it is considered to be a high amount of fillers but is expected to perform the nearest case to ideal Debye response when compared to other ratios. Therefore, it gave near semi-circular shape at high frequency then turned into line at the low-frequency region correlated to conductance loss

due to conductive regions remained by insufficient oxidized graphite [36]. Moreover, the whole ratios seem to perform the same linear trend at low frequency and curved complex dielectric susceptibility at high frequency. It is worth to mention that, the 20% trend is near to circular shape correlated with the highest achieved DiC value which implies good filler capacity and water contents when compared to the other ratios.

CV curve of 20% GO/PVA at different scan rates is shown from 25 to 500 mV^{-1} with a potential window of -1 to 1 V in Fig.2 (a), the capacitance could be estimated using equation 3. The curves show quasi-rectangular shapes indicating double layer behaviour. The capacitance at 25 mV^{-1} is quite matching the values measured by LCR meter and locate in the 10^6 order.

$$C=I/ (dV/dt) \tag{3}$$

, the current I is at V=0 and dV/dt is the scan rate.

The monitored high DiCs values of the GO/PVA composites are in good agreement when considering GO to own super value. However, the composite of low GO weight ratio in PVA was reported to be in the range of several hundred only [24]. [27,28]. Table 1 presents DiC values including pristine GO and GO/polymer blinds in order to show the high diversity of the previously reported results.

Table (1): Dielectric constant of GO materials

Spacer material	DiC value	Reff.
GO	10^4	This work
GO/PVA composite	10^6	
GO/PVA/ polyethylene glycol	10^3	[24]

GO/PVA/ Polypyrrole	10^3	[23]
GO/PVA/ poly (4-styrene sulfonic acid)	10^3	[37]
GO foam	10^2	[32]
GO	pristine (10^1) annealed at 220 °C (10^3)	[27]
GO hybrid sponges	10^2 to 10^3 based on pore size	[36]
GO	10^4	[25]
GO	10^6	[26]

Interestingly, unexpected capacitance decay of the 20% GO/PVA composites was noticed after several weeks. Thereupon, the 20% GO/PVA capacitor was conducted to treatment at 80 °C for 24h in vacuum. After that, the CV characteristics at the previously mentioned parameters of voltage window and scan rate was presented at Fig. 2 (b). The dehydrated CV curves were parallel and symmetry around the x-axis indicating better spacer behaviour than the crude one but with much smaller capacitance values. The estimated capacitance of crude and dehydrated 20% GO/PVA verses scan rates is presented in Fig. 3 (a), where the falling down with higher scan rates is in a steady steeper manner at the dehydrated sample than the crude one, and point to more ideal double plate mode. Ultimately, the estimated DiC dropped drastically and gave a value that is quite comparable to others' reports of GO flakes in PVA [24]. This degradation over time could be attributed to losing water contents, which is presented in the intercalated molecules and adsorbed

quantity due to the high adsorption ability of GO [38]. The impact of water contents on GO dielectric properties was found to increase the (H–O–H) polar molecules [36,39]. On applying an electric field, charge species in water drops will migrate to create dipoles that will be as the size of the drops, which would enhance the dielectric constant. Moreover, the GO intercalated water molecules within the layers could cause enhancement to measured DiC value. On the other hand, PVA encapsulated the GO flakes and prevents it from losing water during the regular dehydration process. In contrast, the low DiC value is gained directly after sufficient dehydration process, long term processing and ageing in spite of encapsulation of polymer, leads to obtaining steady and real DiC composite value. Fig. 3 (b) illustrates the estimated DiC values before and after long term processing effect, the values dropped from 10^6 order to ~88 only at the lowest scan rate. Meanwhile, the two curves showed nearly the same systemic drop without no sharp peaks of low drop upon increasing the applied scan rate. This drastic values transformation showed the crucial impact of water contents and ageing of the spacer dielectric properties.

Fig. (4) present TEM images of the GO and PVA/GO composite, where the GO flakes were proved to be encapsulated and folded with the PVA matrix duo to its high weight ratio and applying facile colloidal technique.

As water contents were proved to play a crucial rule in defining the DiC value of GO/PVA composite, GO spacers will be studied as well in order to investigate the intercalated water molecules impact on dielectric performance. Fig. 5. (a) and (b) represent crude GO and dehydrated GO at 100 °C capacitors CV curves at different scan rates, respectively, where there was an obvious current drop and hence capacitances. The dehydrated GO showed symmetry when compared with the crude one, which indicates enhancement of the spacer dielectric performance after applying dehydration process. There was a high difference of several orders of magnitude of dehydrated

value than crude GO from ~37000 to 25, which is in good agreement with others reports cover both high [25] and low values. The plausible mechanism of GO water impact on the dielectric response is presented in Fig. 5 (c).

In order to investigate heating effect on crude GO and dehydrated GO, XRD was performed and showed in Fig. 6 (a). The oxidized GO sheet is reported to incorporate hydrophilic oxygen functional groups such as carbonyl, carboxyl, hydroxyl and epoxy. It's worth mentioning that, d-spacing of GO layers is associated with the intercalated water content coupled with highly oxidized GO lattice [40]. The chemically prepared crude GO and dehydrated GO exhibited correlated 002 facet peaks centered at $2\theta = 11.31$ ^{o} and 11.93 ^{o}, respectively. The shift is corresponding with reducing the interlayer d_{002} interspacing from 7.82 Å to 7.41 Å by using Bragg's law [41] as a result of applying heat treatments. Despite the slight decreasing value within the interspacing after applying GO dehydration, most of the other water contents except intercalated ones are those adsorbed on the surface and were removed due to the long term process and applied temperature.

According to Seung Hun Huh report [42], the obvious intensity reduction and the increasing of peaks` FWHM could be attributed to defects and nano-holes promoted by mild vaporization of the intercalated H_2O molecules. The estimated dehydrated GO crystals sizes by using Sherrer's equation are reduced after dehydration from ~8.18 nm to 5.92 nm, which is in good agreement with other report [42]. In another hand, the shift of 2θ was be 0.2 ^{o} only in case of composite as presented in Figure S1. Where the presence of polymer shields the shifting of GO.

Raman spectra are shown in Fig. 6 (b) of crude GO and dehydrated GO thin films on glass substrates were measured immediately after treatments without any ageing. Raman spectroscopy is the most reliable method for graphene and GO characterizations [43,44]. Fig.6 (b) shows Raman spectra of crude GO and dehydrated GO. Raman peaks for both samples are centered at 1345.5

(D) and 1584 (G), whereas the dehydrated showed peaks distinction than the crude one that are partially overlapped. I_D/I_G ratio of dehydrated increased to 1.17 than 0.92 for the crude. The dehydrated GO relatively high I_D/I_G ratio could be attributed to many defects formation caused by aggressive chemical oxidation process. The 2D and (D+D`) of crude showed overlapped bump, but the dehydrated showed a well-defined 2D peak at 2692 cm^{-1}.

According to XRD and Raman spectrum analysis, water contents were lost and induced some of defects with limited d-spacing reduction when long term at 100 ^{o}C dehydration process was applied. The dehydration process of GO could be considered as a sort of thermal reduction, which is divided into six main temperature zones, RT−130°C, 140−180°C, 180−600°C, 600−800°C, 800−1000°C, and 1000−2000°C [25]. Within a temperature range of RT−130°C, continuous lattice contraction of GO crystal occurs widely because of mild vaporization of intercalated water molecules. Consequentially, the dehydration process is located in the first region. The decay of GO DiC by heating at mild temperature is reported by Kumar et al. as well [26]. Water losing through this process is responsible for the massive decay of the DiC value as shown in Fig.5 (b). Finally, a low water content GO do not have super DiC value, which is in good agreement with reports of DiC small value [27,28].

Conclusion

Super DiC value in the order of 10^6 was achieved by manufacturing a dielectric spacer based on GO/PVA composite. Electrical analysis showed that the 20% ratio of GO to PVA possess the highest relative dielectric constant. However, 10% GO/PVA composite exhibited the highest quality factor. The observed degradation of the composite DiC over time could be attributed to losing water contents trapped by PVA encapsulation and intercalated molecules inside GO layers. The high dielectric imaginary part and complex permittivity analysis present the composite as a

complex response spacer to the electric field. The hydro response impact on GO and GO/PVA dielectric characteristics caused drastic DiC value drop from 37000 to 25 and from 10^6 to 88, respectively. Accordingly, another crucial parameter that controls the dielectric behaviour of GO-based materials was studied and identify the wide variety of reported values as well.

References

[1]   C.Y. Lu, K.S. Chang-Liao, C.C. Lu, P.H. Tsai, Y.Y. Kyi, T.K. Wang, Investigation of voltage-swing effect and trap generation in high-k gate dielectric of MOS devices by charge-pumping measurement, Microelectron. Eng. 85 (2008) 20–26. doi:10.1016/j.mee.2007.02.012.

[2]   R.M.W. and G.D. Wilk, High dielectric constant materials, Springer, 2005.

[3]   P. Behera, S. Ravi, Effect of Ni doping on structural, magnetic and dielectric properties of M-type barium hexaferrite, Solid State Sci. (2019).

[4]   R. Das, R.N.P. Choudhary, Studies of structural, dielectric relaxor and electrical characteristics of lead-free double Perovskite: Gd2NiMnO6, Solid State Sci. 87 (2019) 1–8.

[5]   Q. Li, F. Liu, T. Yang, M.R. Gadinski, G. Zhang, L. Chen, Q. Wang, Sandwich-structured polymer nanocomposites with high energy density and great charge–discharge efficiency at elevated temperatures, Proc. Natl. Acad. Sci. 113 (2016) 9995–10000. doi:10.1073/pnas.1603792113.

[6]   Z. Spitalsky, D. Tasis, K. Papagelis, C. Galiotis, Carbon nanotube-polymer composites: Chemistry, processing, mechanical and electrical properties, Prog. Polym. Sci. 35 (2010) 357–401. doi:10.1016/j.progpolymsci.2009.09.003.

[7]   D. Cai, M. Song, Recent advance in functionalized graphene/polymer nanocomposites, J. Mater. Chem. 20 (2010) 7906. doi:10.1039/c0jm00530d.

[8]   H. Kim, A.A. Abdala, C.W. MacOsko, Graphene/polymer nanocomposites, Macromolecules. 43 (2010) 6515–6530. doi:10.1021/ma100572e.

[9]   W.-L. Song, Y. Yang, N. Li, Z. Zhou, S. Jiao, D. Fang, H. Chen, Ultra-Lightweight 3D Carbon Current

Collectors: Constructing All-Carbon Electrodes for Stable and High Energy Density Dual-Ion Batteries, Adv. Energy Mater. 8 (2018) 1801439. doi:10.1002/aenm.201801439.

[10]   S. Jiao, G. Zhang, Z. Yu, D.-N. Fang, X. Chen, S. Li, W.-L. Song, H.-S. Chen, T. Teng, J. Tu, Flexible Stable Solid-State Al-Ion Batteries, Adv. Funct. Mater. 29 (2018) 1806799. doi:10.1002/adfm.201806799.

[11]   H. Sun, W. Wang, Z. Yu, Y. Yuan, S. Wang, S. Jiao, A new aluminium-ion battery with high voltage, high safety and low cost, Chem. Commun. 51 (2015) 11892–11895. doi:10.1039/c5cc00542f.

[12]   W. Gao, The chemistry of graphene oxide, Graphene Oxide Reduct. Recipes, Spectrosc. Appl. (2015) 61–95. doi:10.1007/978-3-319-15500-5_3.

[13]   H.H. El-Maghrabi, E.A. Nada, F.S. Soliman, Y.M. Moustafa, A.E.-S. Amin, One pot environmental friendly nanocomposite synthesis of novel TiO2-nanotubes on graphene sheets as effective photocatalyst, Egypt. J. Pet. 25 (2016) 575–584.

[14]   U. Khan, P. May, A. O'Neill, J.N. Coleman, Development of stiff, strong, yet tough composites by the addition of solvent exfoliated graphene to polyurethane, Carbon N. Y. 48 (2010) 4035–4041. doi:10.1016/j.carbon.2010.07.008.

[15]   K. Krishnamoorthy, R. Mohan, S.J. Kim, Graphene oxide as a photocatalytic material, Appl. Phys. Lett. 98 (2011) 2013–2016. doi:10.1063/1.3599453.

[16]   F.L. Jijun Zhao , Lizhao Liu, Graphene Oxide: Physics and Applications, Springer, 2015.

[17]   A.A. Nada, H.R. Tantawy, M.A. Elsayed, M. Bechelany, M.E. Elmowafy, Elaboration of nano titania-magnetic reduced graphene oxide for degradation of tartrazine dye in aqueous solution, Solid State Sci. 78 (2018). doi:10.1016/j.solidstatesciences.2018.02.014.

[18]   H.H. El-Maghrabi, S.M. Abdelmaged, A.A. Nada, F. Zahran, S.A. El-Wahab, D. Yahea, G.M. Hussein, M.S. Atrees, Magnetic graphene based nanocomposite for uranium scavenging, J. Hazard. Mater. 322 (2017). doi:10.1016/j.jhazmat.2016.10.007.

[19]   H.H. El-Maghrabi, A.A. Nada, K.R. Diab, A.M. Youssef, A. Hamdy, S. Roualdes, S. Abd El-Wahab, Facile fabrication of $NiTiO_3$/graphene nanocomposites for photocatalytic hydrogen generation, J.

Photochem. Photobiol. A Chem. 365 (2018). doi:10.1016/j.jphotochem.2018.07.040.

[20] M.T.H. Aunkor, I.M. Mahbubul, R. Saidur, H.S.C. Metselaar, The green reduction of graphene oxide, RSC Adv. 6 (2016) 27807–27828. doi:10.1039/C6RA03189G.

[21] C. Botas, P. Álvarez, C. Blanco, R. Santamaría, M. Granda, P. Ares, F. Rodríguez-Reinoso, R. Menéndez, The effect of the parent graphite on the structure of graphene oxide, Carbon N. Y. 50 (2012) 275–282. doi:10.1016/j.carbon.2011.08.045.

[22] W.S. Hummers, R.E. Offeman, Preparation of Graphitic Oxide, J. Am. Chem. Soc. 80 (1958) 1339–1339. doi:10.1021/ja01539a017.

[23] K. Deshmukh, M.B. Ahamed, S.K.K. Pasha, R.R. Deshmukh, P.R. Bhagat, Highly dispersible graphene oxide reinforced polypyrrole/polyvinyl alcohol blend nanocomposites with high dielectric constant and low dielectric loss, RSC Adv. 5 (2015) 61933–61945. doi:10.1039/C5RA11242G.

[24] K. Deshmukh, M.B. Ahamed, K.K. Sadasivuni, D. Ponnamma, R.R. Deshmukh, S.K.K. Pasha, M.A.A. AlMaadeed, K. Chidambaram, Graphene oxide reinforced polyvinyl alcohol/polyethylene glycol blend composites as high-performance dielectric material, J. Polym. Res. 23 (2016). doi:10.1007/s10965-016-1056-8.

[25] J. Liu, D. Galpaya, M. Notarianni, C. Yan, N. Motta, Graphene-based thin film supercapacitor with graphene oxide as dielectric spacer, Appl. Phys. Lett. 103 (2013) 1–5. doi:10.1063/1.4818337.

[26] K.S. Kumar, S. Pittala, S. Sanyadanam, P. Paik, A new single/few-layered graphene oxide with a high dielectric constant of 106: contribution of defects and functional groups, RSC Adv. 5 (2015) 14768–14779. doi:10.1039/C4RA10800K.

[27] T. Kavinkumar, D. Sastikumar, S. Manivannan, Effect of functional groups on dielectric, optical gas sensing properties of graphene oxide and reduced graphene oxide at room temperature, RSC Adv. 5 (2015) 10816–10825. doi:10.1039/C4RA12766H.

[28] F.C. Salomão, E.M. Lanzoni, C.A. Costa, C. Deneke, E.B. Barros, Determination of High-Frequency Dielectric Constant and Surface Potential of Graphene Oxide and Influence of Humidity by Kelvin Probe

Force Microscopy, Langmuir. 31 (2015) 11339–11343. doi:10.1021/acs.langmuir.5b01786.

[29]   J. Chen, B. Yao, C. Li, G. Shi, An improved Hummers method for eco-friendly synthesis of graphene oxide, Carbon N. Y. 64 (2013) 225–229. doi:10.1016/j.carbon.2013.07.055.

[30]   K.K. Sadasivuni, D. Ponnamma, B. Kumar, M. Strankowski, R. Cardinaels, P. Moldenaers, S. Thomas, Y. Grohens, Dielectric properties of modified graphene oxide filled polyurethane nanocomposites and its correlation with rheology, Compos. Sci. Technol. 104 (2014) 18–25. doi:10.1016/j.compscitech.2014.08.025.

[31]   L. Dissado, Springer Handbook of Electronic and Photonic Materials, in: P.C. S. Kasap (Ed.), Springer Handb. Electron. Photonic Mater., 2017: pp. 219–245. doi:10.1007/978-3-319-48933-9.

[32]   Z.L. Hou, X. Da Liu, W.L. Song, H.M. Fang, S. Bi, Graphene oxide foams: the simplest carbon-air prototypes for unique variable dielectrics, J. Mater. Chem. C. 5 (2017) 3397–3407. doi:10.1039/c6tc04971k.

[33]   P. Debye, Zur Theorie der spezifischen Wärmen, Ann. Phys. 344 (1912) 789–839. doi:10.1002/andp.19123441404.

[34]   N.G. Alexopoulos, R.E. Diazi, W.M. Merrill, Percolation theory in the design of artificial dielectrics, in: IEEE Antennas Propag. Soc. Int. Symp., 1996: pp. 1040–1043. doi:10.1109/aps.1996.549774.

[35]   V.A. Markel, Introduction to the Maxwell Garnett approximation: tutorial, J. Opt. Soc. Am. A. 33 (2016) 1244. doi:10.1364/josaa.33.001244.

[36]   Y. Wang, K.L. Zhang, B.X. Zhang, C.J. Ma, W.L. Song, Z.L. Hou, M. Chen, Smart mechano-hydro-dielectric coupled hybrid sponges for multifunctional sensors, Sensors Actuators, B Chem. 270 (2018) 239–246. doi:10.1016/j.snb.2018.05.023.

[37]   K. Deshmukh, M.B. Ahamed, K.K. Sadasivuni, D. Ponnamma, M.A.A. AlMaadeed, S.K. Khadheer Pasha, R.R. Deshmukh, K. Chidambaram, Graphene oxide reinforced poly (4-styrenesulfonic acid)/polyvinyl alcohol blend composites with enhanced dielectric properties for portable and flexible electronics, Mater. Chem. Phys. 186 (2017) 188–201. doi:10.1016/j.matchemphys.2016.10.044.

[38]   B. Lian, S. De Luca, Y. You, S. Alwarappan, M. Yoshimura, V. Sahajwalla, S.C. Smith, G. Leslie, R.K.

Joshi, Extraordinary water adsorption characteristics of graphene oxide, ArXiv Prepr. ArXiv1707.09502. (2017) 8–11.

[39]   K.L. Zhang, X.D. Cheng, Y.J. Zhang, M. Chen, H. Chen, Y. Yang, W.L. Song, D. Fang, Weather-Manipulated Smart Broadband Electromagnetic Metamaterials, ACS Appl. Mater. Interfaces. 10 (2018) 40815–40823. doi:10.1021/acsami.8b15643.

[40]   H. Jeong, Y.P. Lee, R.J.W.E. Lahaye, M. Park, K.H. An, I.J. Kim, C. Yang, C.Y. Park, R.S. Ruoff, Y.H. Lee, Evidence of Graphitic AB Stacking Order of Graphite Oxides, J. AM. CHEM. SOC. (2008) 155–158. doi:10.1021/ja076473o.

[41]   B.D. Cullity, Elements of X-ray diffraction, 2nd edition, 1978. doi:10.1119/1.1934486.

[42]   S. Hun, Thermal Reduction of Graphene Oxide, in: S. Mikhailov (Ed.), Phys. Appl. Graphene - Exp., InTech, 2011: pp. 73–90. doi:10.5772/14156.

[43]   A. Ferrari, D. Basko, Raman spectroscopy as a versatile tool for studying the properties of graphene, Nat. Nanotechnol. 8 (2013) 235–46. doi:10.1038/nnano.2013.46.

[44]   A.C. Ferrari, J.C. Meyer, V. Scardaci, C. Casiraghi, M. Lazzeri, F. Mauri, S. Piscanec, D. Jiang, K.S. Novoselov, S. Roth, A.K. Geim, Raman spectrum of graphene and graphene layers, Phys. Rev. Lett. 97 (2006) 1–4. doi:10.1103/PhysRevLett.97.187401.
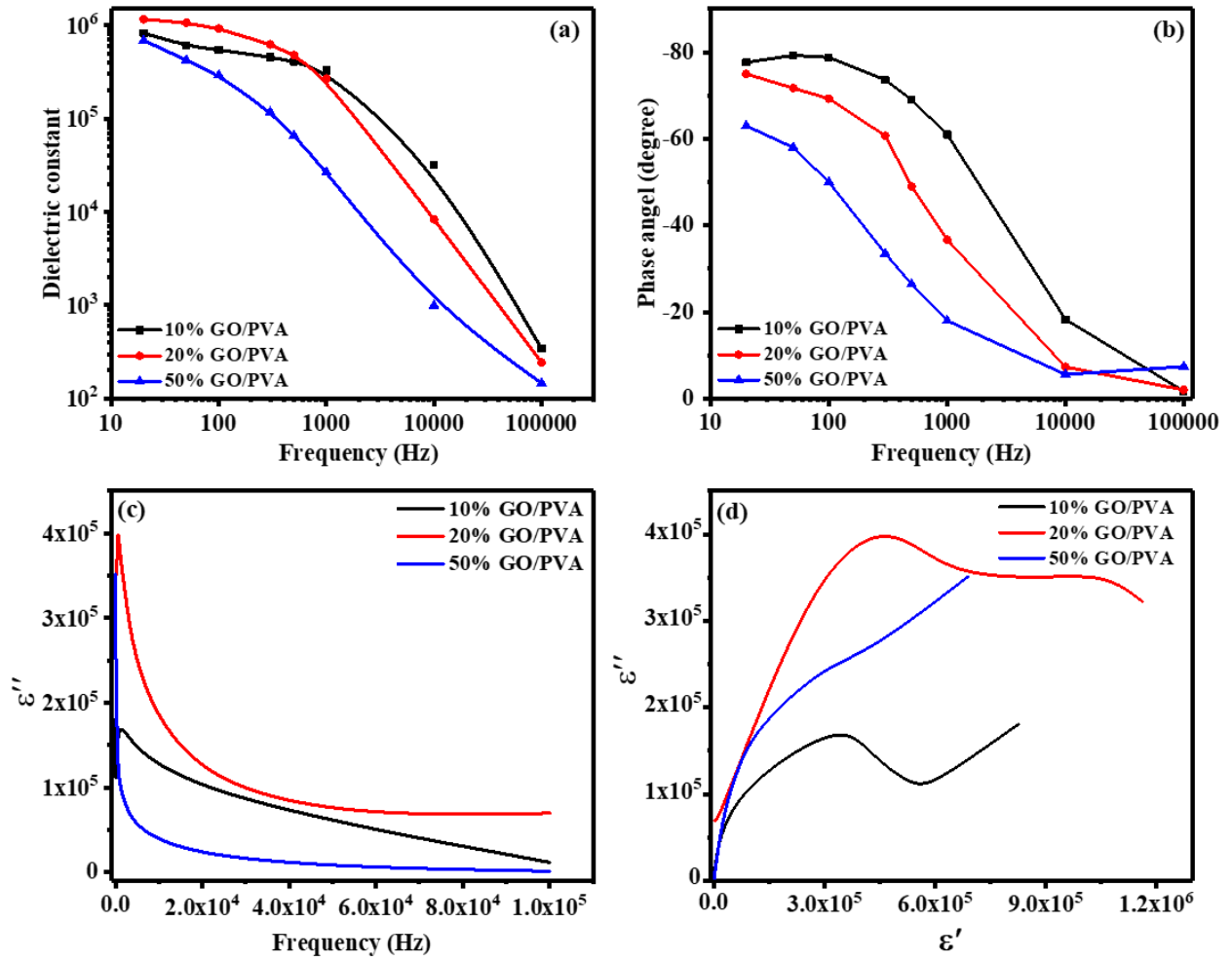
Figure 1. (a) Dielectric real part constants, (b) Phase angle, (c) Dielectric imaginary part, and (d) the complex permittivity Cole-Cole plot. For GO/PVA different weight ratios.
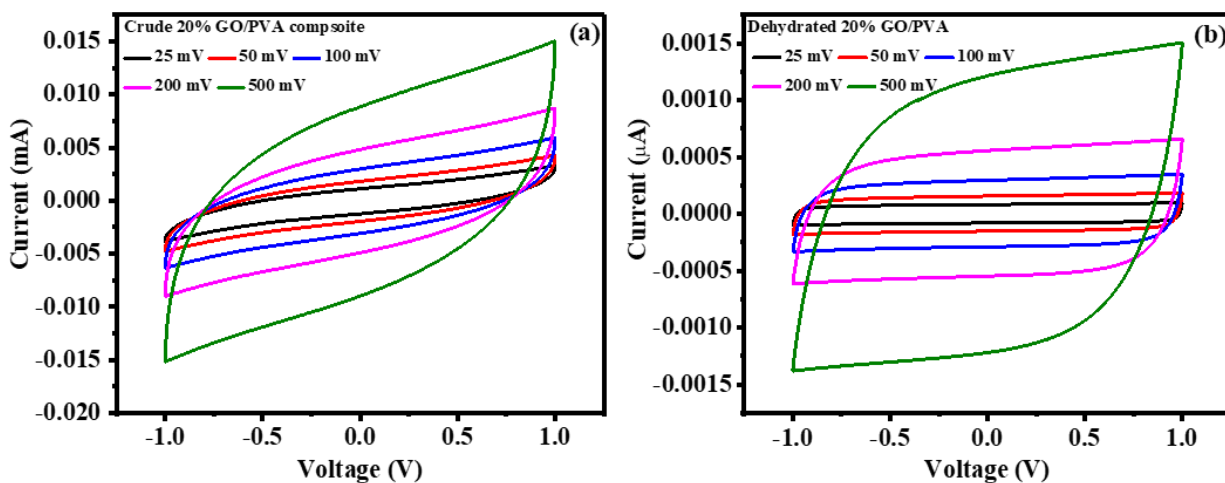
Figure 2. CV curve of crude 20% GO/PVA at different scan rates (a) and CV curve of dehydrated 20% GO/PVA at different scan rates (b).
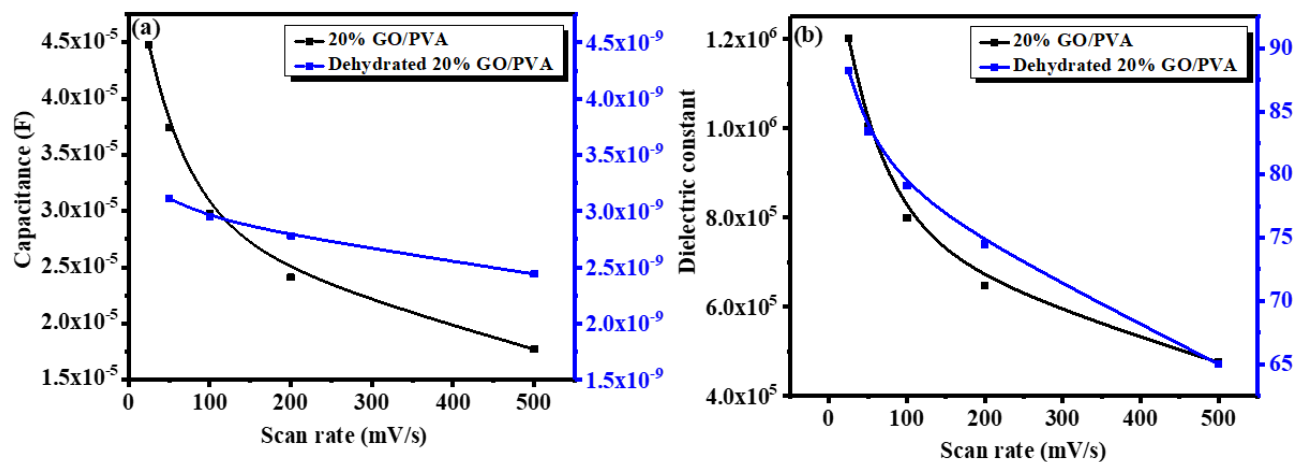

Figure 3. The estimated capacitance (a) and dielectric constant (b) of crude and dehydrated 20% GO/PVA verses scan rates.
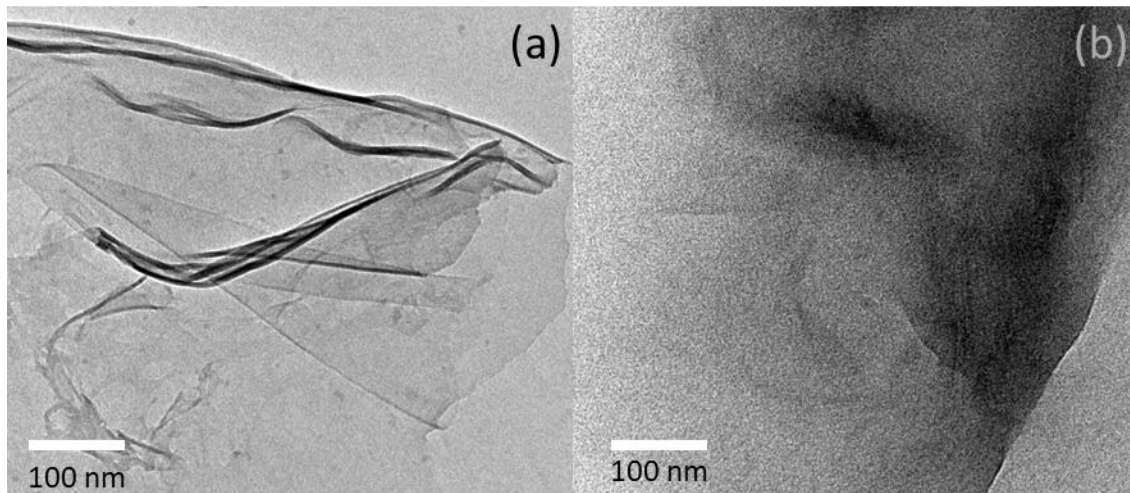
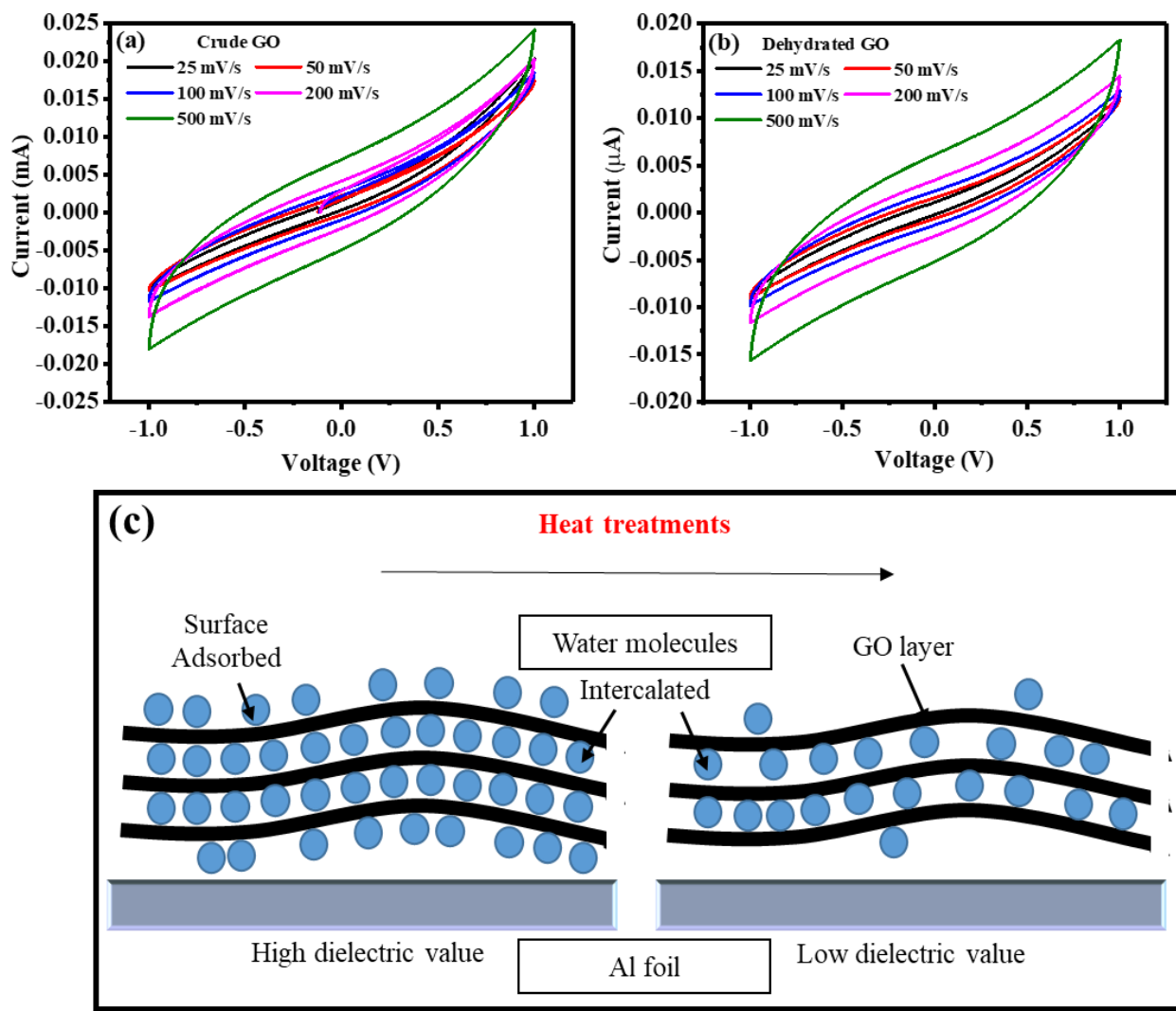Figure 4. TEM images of the GO (a) and PVA/GO composite (b).

Figure 5. CV curves at different scan rates for Crude GO (a), dehydrated GO (b) and the plausible mechanism (c)
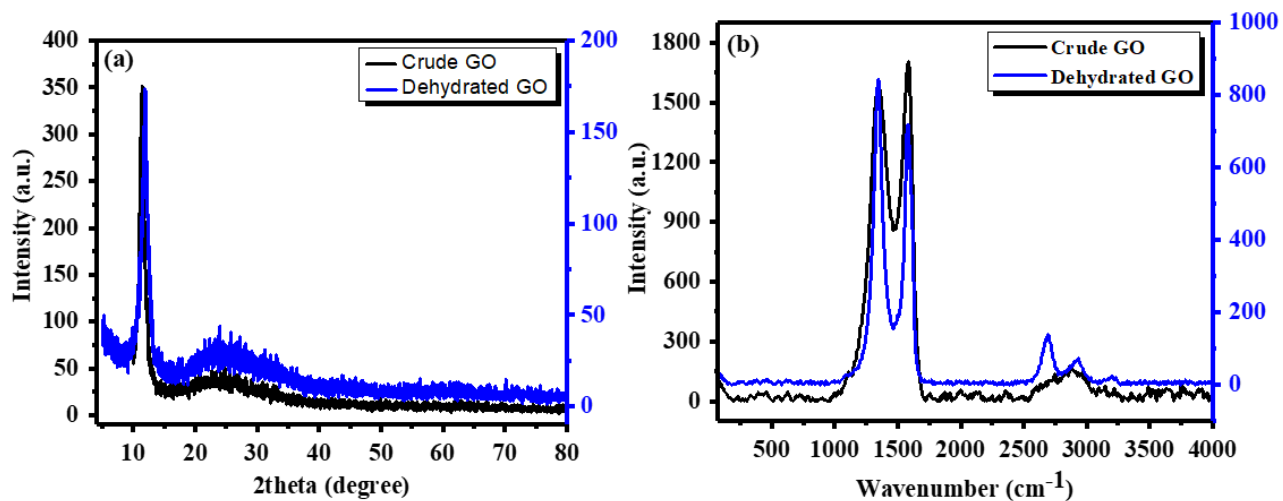
Figure 6. Raman spectra (a) and XRD (b) of crude GO and dehydrated GO thin films on glass substrates.